

1 **Full title:** Protein lactylation induced by neural excitation

2 **Short title:** Protein lactylation in the brain

3 **Authors:** Hideo Hagihara¹, Hirotaka Shoji¹, Hikari Otabi^{2,3}, Atsushi Toyoda^{2,3,4}, Kaoru Katoh⁵,
4 Masakazu Namihira⁵, Tsuyoshi Miyakawa^{1*}

5 **Affiliations:**

6 ¹ Division of Systems Medical Science, Institute for Comprehensive Medical Science,
7 Fujita Health University, Aichi, Japan

8 ² College of Agriculture, Ibaraki University, Ibaraki, Japan

9 ³ United Graduate School of Agricultural Science, Tokyo University of Agriculture and
10 Technology, Tokyo, Japan

11 ⁴ Ibaraki University Cooperation between Agriculture and Medical Science (IUCAM),
12 Ibaraki, Japan

13 ⁵ Biomedical Research Institute, National Institute of Advanced Industrial Science and
14 Technology (AIST), Ibaraki, Japan

15 *Corresponding Author: Tsuyoshi Miyakawa (miyakawa@fujita-hu.ac.jp)

16 **Keywords:** lactylation, lactate, brain, posttranslational modification, histone H1

17

18 ORCID ID

19 Hideo Hagihara: <https://orcid.org/0000-0001-9602-9518>

20 Hiroataka Shoji: <https://orcid.org/0000-0003-4843-6949>

21 Hikari Otabi: <https://orcid.org/0000-0001-5127-8190>

22 Atsushi Toyoda: <https://orcid.org/0000-0002-0245-3244>

23 Kaoru Katoh: <https://orcid.org/0000-0001-6590-413X>

24 Masakazu Namihira: <https://orcid.org/0000-0003-2108-5712>

25 Tsuyoshi Miyakawa: <https://orcid.org/0000-0003-0137-8200>

26 **Abstract**

27 Lactate is known to have diverse roles in the brain at the molecular and behavioral levels
28 under both physiological and pathophysiological conditions, such as learning and memory
29 and regulation of mood. Recently, a novel post-translational modification called lysine
30 lactylation has been found in histone H3 of mouse macrophages, and the lactylation levels
31 paralleled the intracellular lactate levels¹. However, it is unknown whether lysine lactylation
32 occurs in brain cells, and if it does, whether lactylation is induced by the stimuli that
33 accompany changes in lactate levels. Herein, we reveal that lysine lactylation in brain cells
34 is regulated by systemic changes in lactate levels, neural excitation, and behaviorally
35 relevant stimuli. Lysine lactylation levels were increased by lactate treatment and by high-
36 potassium-induced depolarization in cultured primary neurons; these increases were
37 attenuated by pharmacological inhibition of monocarboxylate transporter 2 and lactate
38 dehydrogenase, respectively, suggesting that both cell-autonomous and non-cell-
39 autonomous neuronal mechanisms are involved in overall lysine lactylation. *In vivo*,
40 electroconvulsive stimulation increased lysine lactylation levels in the prefrontal cortices of
41 mice, and its levels were positively correlated with the expression levels of the neuronal
42 activity marker c-Fos on an individual cell basis. In the social defeat stress model of
43 depression in which brain lactate levels increase, lactylation levels were increased in the
44 prefrontal cortices of the defeated mice, which was accompanied by increased c-Fos
45 expression, decreased social behaviors, and increased anxiety-like behaviors, suggesting

46 that stress-induced neuronal excitation may induce lysine lactylation, thereby affecting
47 mood-related behaviors. Further, we identified 63 candidate lysine-lactylated proteins in
48 the mouse cortex and found that lactylation levels in histone H1 increased in response to
49 defeat stress. This study may open up an avenue for exploration of a novel role of neuronal
50 activity-induced lactate mediated by protein lactylation in the brain.

51 **Main text**

52 Lactate in the brain has emerged as an energy substrate and a valuable signaling molecule²,
53 and its alteration has been implicated in multiple neuropsychiatric disorders. Among
54 various strains/conditions of animal models of neuropsychiatric disorders, we have
55 identified more than 20 out of 65 strains/conditions of mice that show altered lactate levels
56 in whole brain^{3,4}. A recent research identified lysine lactylation (Kla) as a novel post-
57 translational modification in histone protein that can be stimulated by lactate¹. A report by
58 Zhang et al. suggested that histone H3 Kla mediates a metabolic alteration-related lactate
59 regulation of gene expression in mouse bone marrow-derived macrophages¹. The following
60 reports have described key roles of lactate-induced Kla in macrophages in the transition of
61 macrophages from a proinflammatory state to a reparative state⁵ and the pathogenesis of
62 lung fibrosis⁶. However, it has not been elucidated whether this Kla occurs and is regulated
63 by exogenous lactate treatment or by stimulation that increases endogenous lactate levels
64 in other types of cells/tissues including brain cells.

65

66 **Lactate treatment and neuronal excitation increase protein lactylation in the brain**

67 Kla was detected by western blot analysis in mouse brain tissues, with patterns different
68 from those observed in macrophages and peripheral organs (Fig. 1a, Extended Data Fig. 1).
69 With confocal microscopic imaging, we observed Kla signals throughout the cell, including
70 somata and neurites, with a relatively weak signal in the nucleus region in primary cultured
71 neurons expressing the neuronal marker β III-tubulin (Fig. 1b). These results suggest that Kla
72 modifications occur in various proteins to varying degrees, potentially with neural cell-
73 specific functional roles different from those found in macrophages.

74 We investigated whether extracellular application of lactate stimulates Kla in
75 neuronal cells as seen in macrophages¹. Lactate treatment significantly increased Kla
76 immunoreactivity in the primary cultured neurons (Fig. 1c, d), as confirmed by an
77 independent experiment performed at a different institute (Extended Data Fig. 2). The
78 increase in Kla immunoreactivity was attenuated in a dose-dependent manner by α -cyano-
79 4-hydroxycinnamate (4-CIN), a monocarboxylate transporter 2 (MCT2) inhibitor that blocks
80 lactate transport into neurons (Fig. 1d). Considering that there are few astrocyte-like cells

81 in the culture (Fig. 1e), lactate derived from astrocytes may minimally affect the lactate
82 contents therein. Furthermore, in an *in vivo* experiment, we found that chronic and
83 systemic treatment with lactate, shown to increase extracellular lactate concentrations in
84 the brain⁷, increased K1a immunoreactivity in the mouse prefrontal cortex (PFC) (Fig. 1f–h),
85 but not in the hippocampus (Extended Data Fig. 3), suggesting that exogenous lactate
86 stimulates protein lactylation in the brain in a region-dependent manner.

87 To examine in what neural cell types protein lactylation occurs in the brain, we
88 conducted double-immunostaining of K1a with cell type-specific markers on mouse PFC:
89 Camk2a for glutamatergic neurons, GAD67 for GABAergic neurons, S100b for astrocytes,
90 and CD68 for microglia. K1a immunoreactivity was found in all cell types examined,
91 suggesting that protein lactylation may ubiquitously occur in neural cells in the brain (Fig.
92 1i).

93

94 **Neuronal excitation stimulates protein lactylation in the brain**

95 Neuronal excitation increases brain lactate levels^{8–12}. We examined lactate and protein
96 lactylation levels using an *in vitro* neuronal excitation model. Primary neuron cultures were
97 treated with a high concentration of potassium ions (high-K) (Fig. 2a) to induce
98 depolarization of neurons *in vitro*. The high-K treatment resulted in increased lactate
99 concentration in the culture supernatant at 30 minutes after the initiation of treatment (Fig.
100 2b). The intracellular lactate level showed a trend of time-dependent increase and reached
101 significant increase at 2 hours after the initiation of high-K treatment (Fig. 2b). The high-K-
102 induced increase in K_{1a} levels was attenuated by treatment with sodium oxamate (OX),
103 which inhibits lactate dehydrogenase (LDH) activity in neural^{13,14} and other cell types¹ (Fig.
104 2c), suggesting that neuronal excitation may induce protein lactylation via intracellular
105 metabolism and the glycolytic pathway. To test this hypothesis *in vivo*, we treated mice with
106 electroconvulsive stimulation (ECS) and then examined lactate and protein lactylation levels
107 in the brain. The brain lactate levels increased 10 minutes after ECS and persisted for 1 hour
108 (Fig. 2d, e). We then examined K_{1a} levels in mouse brains treated with ECS in combination
109 with OX and/or 4-CIN (Fig. 2f). While the ECS-induced increase in K_{1a} immunoreactivity was

110 not significantly affected by prior treatment with either OX or 4-CIN alone, it was attenuated
111 by a combination treatment with OX and 4-CIN (Fig. 2g, h), suggesting that, *in vivo*, both
112 intracellular new lactate production and extracellular lactate uptake have a role in neuronal
113 activation-induced protein lactylation in the acute phase.

114 c-Fos is an immediate early gene product used as a marker for neuronal
115 activation¹⁵. Utilizing the characteristics of c-Fos expression, we investigated the relation
116 between Kla and c-Fos expressions in the ECS mouse model. Upon double-immunostaining
117 analysis of c-Fos-expressing cells in the PFC, we found a significant positive correlation
118 between Kla and c-Fos immunoreactive intensities on an individual cell basis level (Fig. 2i, j,
119 Extended Data Fig. 4). Considering that intensity of electrical stimulation positively
120 correlates with c-Fos-labeling levels in individual neurons¹⁶, our results suggest that the
121 more neurons are activated, the more Kla is induced in the cells. However, we have to note
122 that there also are many cells that are Kla-positive but c-Fos-negative, suggesting that some
123 Kla formations are independent of neuronal activation or lasts longer than that of c-Fos
124 protein expression after neuronal activation.

125

126 **Social stress stimulates protein lactylation in the brain**

127 We explored whether protein lactylation in the brain is modified by a physiologically
128 relevant stimulus using a social defeat stress (SDS) model of depression. SDS has been
129 shown to increase c-Fos expression levels in many brain regions^{17–19}. Brain lactate levels
130 increased immediately (10 minutes) after a single exposure to the stress, and the increase
131 was attenuated by prior treatment with OX¹ (Extended Data Fig. 5).

132 Further, we conducted a chronic experiment where the mice experienced daily
133 defeat stress with prior treatment with OX or vehicle (saline) for 10 consecutive days. To
134 examine the correlation between brain lactate and K1a levels and behavioral measures of
135 anxiety and depression, we conducted a series of behavioral tests prior to brain sampling
136 (Fig. 3a, Extended Data Fig. 6, 7). In the social avoidance test, the social interaction ratio
137 decreased in both chronic vehicle-treated and OX-treated socially defeated mice compared
138 to control mice (Fig. 3b). Based on the standard criteria^{20,21}, we focused on mice susceptible

139 to SDS, which showed a social interaction ratio <1 in the social avoidance test and
140 designated them as defeated mice for the following behavioral and brain tissue analyses.

141 We found that brain lactate levels were higher in defeated mice than in control
142 mice (Fig. 3c), as confirmed by independent sets of mice (Extended Data Fig. 8). Brain lactate
143 levels were paradoxically increased in OX-treated defeated mice at 9 days after the last
144 stress exposure and OX treatment compared to vehicle-treated defeated mice and control
145 mice (Fig. 3c). Simple correlation (Fig. 3d; Extended Data Fig. 9) and multiple regression
146 (Extended Data Table 1) analyses suggested that increased brain lactate levels are
147 preferentially associated with increased anxiety-like behaviors. In this stress model, Kla
148 levels in the PFC were increased in vehicle-treated defeated mice and, to a larger extent, in
149 OX-treated defeated mice compared to control mice (Fig. 3e, f).

150 Expression of neuronal activity marker c-Fos in the PFC also increased in vehicle-
151 treated defeated mice and, to a larger extent, in OX-treated defeated mice, in both a familiar
152 environment in the home cage (non-stimulated basal condition) and novel environment
153 exposed to the open field (condition with anxiogenic stimulation) (Fig. 3g, h). In the mice

154 that received anxiogenic stimulation to ensure more c-Fos-expressing cells, we found that
155 the Kla level positively correlated with the c-Fos expression level in the PFC (Fig. 3i).
156 Although changes in Kla and c-Fos expression levels were observed in some other brain
157 regions implicated in anxiety and depression behaviors (e.g., hippocampus, lateral habenula,
158 and amygdala; Extended Data Fig. 10, 11), no significant correlations were found between
159 Kla and c-Fos expression levels in brain regions other than the PFC (Extended Data Fig. 12),
160 suggesting that simultaneous induction of c-Fos and Kla occurs in a brain region-specific
161 manner following repeated SDS. Furthermore, we found that Kla levels in the PFC, but not
162 in the amygdala and hippocampal subregions, negatively correlated with the social
163 interaction ratio in the social avoidance test (Fig. 3j, Extended Data Fig. 13) and with
164 distance traveled in the dark compartment in the light–dark transition test (Fig. 3k),
165 indicating that the more susceptible to SDS and the more anxious the mouse is, the higher
166 the Kla levels in the PFC.

167

168 **Identification of lactylated proteins in the brain**

169 We sought to identify and quantify the brain proteins modified by lactylation and whose
170 lactylation levels changed in response to SDS. Accordingly, we analyzed the PFC of defeated
171 and control mice using Kla antibody immunoprecipitation and mass spectrometry
172 techniques. This analysis identified 63 candidate lysine-lactylated proteins in the mouse PFC
173 (Extended Data Table 2). GO-enrichment analysis with DAVID^{22,23} showed that these
174 proteins were mainly enriched in nucleosome- and histone-related biological processes
175 (Extended Data Table 3). Among them, 12 proteins were suggested to be changed by SDS,
176 of which seven were upregulated and five were downregulated. Notably, four subtypes of
177 histone H1 were included in the 12 changed proteins and all were upregulated, suggesting
178 that SDS increases lactylation at histone H1. We confirmed these observations by
179 conducting immunoprecipitation with the histone H1 antibody followed by western blot
180 analysis with the Kla antibody (Extended Data Fig. 14). In the PFC, 59.5% of cells were
181 positive for histone H1 and nearly all the histone H1-positive cells (94.6%) were Kla positive,
182 and vice versa (99.1% of Kla-positive cells were histone H1 positive) (Fig. 4a, b). Upon super-
183 resolution imaging using stimulated emission depletion (STED) microscopy, we observed

184 histone H1 and Kla double-positive structures in the nucleus, suggestive of lysine lactylation
185 at histone H1 (Fig. 4c). Importantly, the double-positive structures in the nucleus increased
186 in the defeated mice compared to control mice (Fig. 4d), further supporting that SDS
187 enhances lysine lactylation levels at histone H1 in the PFC.

188

189 **Discussion**

190 In this study, we showed that a novel post-translational modification called lysine
191 lactylation occurs in brain cells and that its levels can be changed by neuronal excitation.
192 We found that increasing lactate levels by lactate addition or inducing neuronal excitation
193 with high-K or ECS increased Kla levels in the mouse brain cells both *in vitro* and *in vivo*. The
194 lactate and Kla levels also increased by behaviorally induced neuronal excitation associated
195 with SDS. In the SDS model of depression, Kla levels in the PFC, a core brain region
196 implicated in depressive and anxiety disorders, correlated with anxiety-like behaviors,
197 suggesting a potential behavioral significance of Kla in the brain. Furthermore, our

198 proteomic approach identified 63 candidate lactylated proteins in the mouse PFC and
199 highlighted that histone H1 lactylation increases in response to chronic stress.

200 Our results using SDS model mice suggest that, in stress-related pathological
201 conditions, excess neuronal activity may underlie increased protein lactylation in the PFC,
202 potentially associated with susceptibility to stress and anxiety-like behavior, although the
203 causal mechanism remained unclear. Given that increased Kla levels reflect neuronal
204 activity, it might be expected that significant correlations can be seen between Kla levels in
205 the brain regions other than PFC and behavioral alterations. Adaptation in neuronal activity
206 has been suggested to occur following repeated SDS in some brain regions; for example,
207 neurons in the central nucleus of amygdala became less active and showed suppressed c-
208 Fos expression after repeated SDS²⁴. Such adaptation in neuronal activity may affect c-Fos
209 expression, possibly as well as Kla induction, resulting in no clear correlations between
210 behavior and Kla levels in brain regions other than the PFC.

211 Regarding the mechanisms of Kla formation, Zhang et al. showed that, using a ¹³C-
212 labeled L-lactate incorporation method, Kla could be derived directly from lactate

213 exogenously applied to mouse bone marrow-derived macrophages¹. Conversely, other
214 studies have suggested that K_{la} formation could be mediated indirectly by a glycolytic
215 intermediate, lactoylglutathione, which can provide a lactyl group to lysine residues. L-
216 Lactate is suggested to suppress the activity of glyoxalase 2, an enzyme catalyzing the
217 conversion of lactoylglutathione into glutathione and free D-lactate. Such suppression due
218 to increased L-lactate could elevate lactoylglutathione levels, which in turn, may facilitate
219 the indirect lactylation pathway. Gaffney et al. used a stable isotope labeling of amino acids
220 in cell culture (SILAC) model to identify lactylated proteins that could be formed via
221 lactoylglutathione in the HEK293 cell line²⁵. The identified proteins were enriched in
222 glycolytic and carbon-metabolism enzymes but did not include histone family proteins. As
223 mentioned above, K_{la} forms directly from lactate on histone H3¹. Our list includes histone
224 H3 as well as the 60S ribosomal protein L30 and Rho guanine nucleotide exchange factor 2,
225 also found in the 350-protein list published by Gaffney et al.²⁵ These observations suggest
226 that direct and indirect lactylation pathways may coexist, rather than being exclusive,

227 depending on the proteins expressed in the brain. Regardless of the mechanisms, lysine
228 lactylation may play a role in coupling metabolic changes to gene-expression regulation.

229 Our analyses highlighted that H1 histones increase their K1a levels in response to
230 SDS. Histone H1 is known to be a linker histone, having a key role in higher-order chromatin
231 folding and genome stability. Seven subtypes of H1 histone have been identified in
232 mammalian somatic cells, i.e., H1.0–1.5 and H1.10²⁶. Numerous post-translational
233 modifications have been identified in H1, such as phosphorylation, methylation, acetylation,
234 formylation, crotonylation, and citrullination²⁷. Post-translational modifications of histone
235 H1 have received less attention than those of core histones; therefore, knowledge on the
236 functional role of H1 modifications is limited^{26,28}, especially in brain cells. In the case of
237 mouse macrophage histone H3, lactylation competes with acetylation at lysine residues to
238 regulate the expression of a specific gene set. Extrapolating these findings to histone H1
239 and considering that histone H1 acetylation regulates chromatin compaction and
240 decondensation and hence the accessibility of linker DNA regions to transcription factors,

241 histone H1 lactylation may also be involved in gene-expression regulation depending on the
242 balance of K_{la} with acetylation.

243 In conclusion, this study indicates that a novel post-translational modification
244 called lysine lactylation occurs in the brain, and it is regulated by neuronal activity. While
245 63 candidate lactylated proteins were identified in the brain, it remains unclear whether
246 such a modification has functional significance for each protein at the cellular and behavior
247 levels, and if it does, in what brain regions and in what cell types and in what types of
248 behavioral phenotypes. It would also be interesting to explore whether protein lactylation
249 in the brain is related to the etiology and pathophysiology of neuropsychiatric disorders, as
250 are altered lactate levels in the brains of animals³. Further studies may reveal unknown
251 roles of lactate, linking neural activity, glycolytic metabolism, and molecular signaling
252 mediated by protein lactylation under physiological and pathophysiological conditions.

253

254 **Methods**

255 **Animals**

256 C57BL/6J mice (7–9 weeks old) were purchased from Charles River Laboratories Japan, Inc.

257 (Hino, Japan) and Japan SLC (Shizuoka, Japan). Retired ICR mice were purchased from Chubu

258 Kagaku Shizai Co. Ltd. (Nagoya, Japan) and Japan SLC. The mice were habituated to their

259 environments for a week before experimentation. All animal experiments were approved

260 by the Institutional Animal Care and Use Committee of Fujita Health University, Ibaraki

261 University, and The National Institute of Advanced Industrial Science and Technology based

262 on the Law for the Humane Treatment and Management of Animals and the Standards

263 Relating to the Care and Management of Laboratory Animals and Relief of Pain. Every effort

264 was made to minimize the number of animals used.

265

266 **Cell culture**

267 Embryonic C57BL/6J mice (15.5–16.5 days old) were used for primary neuron culture. The
268 frontal cortices and hippocampi were dissected from the brains in cold HEPES-buffered,
269 calcium and magnesium-free Hank's balanced salt solution (HBSS; 14175-103, Thermo
270 Fisher Scientific, Waltham, MA, USA) and dissociated in HBSS containing 0.25% papain
271 (LS003127, Worthington Biochemical Corporation, Lakewood, NJ, USA), 0.1% L-cysteine
272 (C7352, Merck, Darmstadt, Germany), 0.1% bovine serum albumin (BSA; A2153, Merck),
273 and 0.01% DNase I (D4263, Merck) at 37°C for 12 minutes. The enzymatic digestion was
274 stopped by adding a plating medium (Dulbecco's modified Eagle medium, D5796, Merck,
275 containing 10% fetal bovine serum). Tissues were dissociated by pipetting, centrifuged at
276 room temperature for 10 minutes, and resuspended in the plating medium. Cells were
277 counted, seeded at a density of 25,000 cells/cm² on culture plates or glass coverslips
278 previously coated with 0.01% poly-L-lysine (P8920, Merck), and incubated at 37°C. After 2
279 hours, the plating medium was replaced by a culture medium (Neurobasal™ medium
280 [21103-049, Thermo Fisher Scientific] containing B-27™ Supplement [17504-044, Thermo
281 Fisher Scientific], 0.5 mM L-glutamine [G7513, Merck], and 1% penicillin-streptomycin

282 solution [P4333, Merck]). The culture medium was changed by one half with fresh medium
283 every 3–4 days. At 10–14 days *in vitro*, drug treatment experiments, immunocytochemical
284 analysis were conducted.

285

286 **Immunocytochemistry**

287 Cells were fixed with 4% paraformaldehyde (PFA) in phosphate-buffered saline (PBS) for 10
288 minutes, pre-incubated for 30 minutes in 5% BSA (Merck) in PBS containing 0.05% Tween-
289 20 (PBST), and then incubated for 30 minutes in PBS containing the primary antibodies:
290 rabbit polyclonal anti-lactyllysine antibody (PTM-1401, PTM Biolabs, Hangzhou, China),
291 mouse monoclonal anti-tubulin β 3 (801201, BioLegend, San Diego, CA, USA), and mouse
292 monoclonal anti-glial fibrillary acidic protein antibody (G3893, Sigma-Aldrich, St Louis, MO,
293 USA). Immunoreactivity to the antigen was visualized using Alexa Fluor 488- and Alexa Fluor
294 594-conjugated secondary antibodies (Molecular Probes, Eugene, OR). Nuclear staining was
295 performed with Hoechst 33258 (Polysciences, Warrington, PA). All reactions were
296 performed at room temperature. We used a microscope (LSM 510 META; Zeiss, Göttingen,

297 Germany) to obtain images of the stained cells. The soma of tubulin β 3-positive cells was
298 manually delineated and the signal intensity of Kla staining within the region of interest was
299 recorded using ZEN software (Zeiss). At least 200 cells from triplicate wells per condition
300 were analyzed.

301 The specificity of the Kla antibody was confirmed using dot blot analysis of lysine
302 residues with various types of modifying groups (i.e., acetyl-, crotonyl-, propionyl-, butyryl-,
303 trimethyl-, and succinyl-lysine); the antibody showed almost no cross-reactivity with these
304 modified lysine residues^{1,29}. Additionally, lactate treatment dramatically increased Kla
305 immunoreactivity in human MCF-7, Hela, and MDA-MB-231 cell lines^{1,29}.

306

307 **Immunohistochemistry**

308 Immunohistochemical analysis was performed as previously described with some
309 modifications^{30,31}. Briefly, mice were deeply anesthetized with isoflurane and transcardially
310 perfused with PBS followed by 4% PFA in PBS. The brains were dissected, immersed
311 overnight in the same fixative, and cryoprotected by sequential incubation in 10, 20, and

312 30% sucrose in PBS for 2–3 days each at 4°C. After cryoprotection, brains were mounted in
313 Tissue-Tek optimal cutting temperature compound (Miles, Elkhart, IN), frozen, and cut into
314 30- μ m-thick coronal sections using a microtome (CM1850; Leica Microsystems, Wetzlar,
315 Germany). The sections were stored in PBS containing 0.1% sodium azide at 4°C until further
316 use. The sections were pre-incubated for 1 hour at room temperature in 5% skim milk in
317 PBST and then incubated overnight at 4°C in PBS containing the primary antibodies. We
318 used rabbit polyclonal anti-lactyllysine antibody (PTM-1401, PTM Biolabs), mouse
319 monoclonal anti-CaM Kinase II α subunit antibody (05-532, Merck), mouse monoclonal anti-
320 GAD67 antibody (MAB5406, Millipore), mouse monoclonal anti-S-100 β subunit antibody
321 (S2532, Merck), rat monoclonal anti-CD68 antibody (ab53444, abcam), and mouse
322 monoclonal anti-c-Fos antibody (sc-166940, Santa Cruz Biotechnology, Santa Cruz, CA, USA).
323 For c-Fos staining, antigen retrieval was performed by autoclave heating at 120°C for 1
324 minute in 0.01 M sodium citrate buffer prior to the blocking step. Immunoreactivity to the
325 antigen was visualized using Alexa Fluor 488- or Alexa Fluor 594-conjugated secondary
326 antibody (Molecular Probes). Nuclear staining was performed with Hoechst 33258

327 (Polysciences). We used a microscope (LSM 510 META; Zeiss) to obtain images of the
328 stained sections. Three to seven sections from each animal were processed for semi-
329 quantification analyses in each brain region, and the averaged values were considered as
330 one sample. c-Fos-positive cells were counted in the indicated brain regions, manually
331 delineated using ZEN software (Zeiss) according to the mouse brain atlas³². For c-Fos and
332 Kla immunofluorescence intensity analysis in individual cells, c-Fos-positive cells were
333 circled, and the signal intensity for each antibody within the circled areas was recorded
334 using Zen software (Zeiss). For Kla immunofluorescence intensity, to reduce potential
335 artifacts across sections, the values were calculated from the mean signal intensity of the
336 entire image by subtracting background signals using Zen software (Zeiss). Semi-
337 quantification analyses were performed in the medial PFC (approximately from 2.1 to 2.4
338 mm from the bregma), dorsal hippocampus, lateral habenula, and amygdala (approximately
339 from -2.1 to -1.6 mm from the bregma), and ventral hippocampus (approximately from -3.5
340 to -3.8 mm from the bregma).

341

342 **STED microscopy**

343 Brain slices were doubleimmunostained as described above. Mouse monoclonal anti-
344 histone H1 antibody (sc-8030; Santa Cruz Biotechnology, Inc.) and rabbit polyclonal anti-Kla
345 antibody were the primary antibodies, and Alexa Fluor 555- and Alexa Fluor 488 conjugated
346 antibodies (Molecular Probes) were the secondary antibodies.

347 STED images were acquired with a TCS SP8 STED 3X system (Leica Microsystems,
348 Wetzlar, Germany) with 2ch HyDSMD detectors³³. A white laser (for excitation) and a 660-
349 nm laser with a donut beam (for stimulated emission depletion) were used for STED imaging.
350 For detection of histone H1 and Kla, we used excitation wavelengths of 561 and 488 nm,
351 respectively. Raw STED images (pixel size: 20 nm) were recorded with a 93× glycerol
352 immersion objective (Leica HC PL APO 93×/1.30 GLYC motC STED W) and deconvoluted
353 using the Huygens software (SVI, Hilversum, Netherlands). The percentage of merged area
354 in a nucleus stained for both histone H1 and Kla was estimated using the ImageJ program.

355

356 **Immunoprecipitation**

357 The PFCs were dissected, snap-frozen in liquid nitrogen, and stored at -80°C until further
358 use. Fifty microliters of Dynabeads™ Protein G solution (10007D; Thermo Fisher Scientific)
359 was separated into low-protein absorption tubes (PROKEEP; Watson Bio Lab, Tokyo, Japan)
360 and reacted with 2 µg of rabbit polyclonal anti-lactyllysine antibody (PTM Biolabs) or normal
361 rabbit IgG (Cell Signaling Technology, Inc., Danvers, MA, USA). The frozen tissues were then
362 homogenized in lysis buffer (FNN0021, Thermo Fisher Scientific). Then, 200 µL of 1-µg/µL
363 tissue lysate was added to the bead-antibody complex and incubated with a rotation of 30
364 minutes at room temperature. The bead-antibody-antigen complex was then processed for
365 mass spectrometry.

366

367 **Mass spectrometry**

368 *Trypsin digestion:* Bead-antibody-antigen complex was washed with 50 mM ammonium
369 bicarbonate. The binding proteins were eluted by trypsin (Promega Corporation, Madison,
370 WI, USA) for 1 hour at 37°C, reduced with 10 mM dithiothreitol for 30 minutes at room
371 temperature, and alkylated with 20 mM iodoacetamide for 30 minutes at room

372 temperature, followed by an overnight incubation at 37°C. Digestion was stopped by adding
373 trifluoroacetic acid. The digested sample was desalted using GL-Tip SDB (GL Sciences, Tokyo,
374 Japan) and then dissolved in 20 µL of 0.1% trifluoroacetic acid.

375 *Liquid chromatograph-tandem mass spectrometer (LC-MS/MS) analysis:* The peptides were
376 analyzed using LC-MS (EASY-nLC™ 1000, Orbitrap Fusion EDT; Thermo Fisher Scientific).
377 Injected peptides were trapped on an Acclaim™ PepMap™ 100 C18 LC column (3 µm particle
378 size, 0.075 mm inner diameter × 20 mm length; Thermo Fisher Scientific) and separated on
379 an EASY-Spray LC column (3 µm particle size, 0.075 mm inner diameter × 150 mm length;
380 Thermo Fisher Scientific) with a linear gradient of 0–35% acetonitrile with 0.1% formic acid
381 over 60 minutes at a flow rate of 300 nL/minute. Data acquisition was performed using
382 Xcalibur™ (Thermo Fisher Scientific). Full MS spectra (m/z 375–1500) were acquired at a
383 resolution of 120,000. The most intense precursor ions were selected for collision-induced
384 fragmentation in the linear ion trap at a normalized collision energy of 35%. Dynamic
385 exclusion was employed within 60 seconds to prevent repetitive selection of peptides.

386 *Data analysis:* Raw data were analyzed using Proteome Discoverer™ (version 2.2, Thermo
387 Fisher Scientific) with the Mascot search engine (version 2.6.1, Matrix Science Ltd., London,
388 UK) against the Swiss-Prot database. The search parameters were as follows: mass
389 tolerances in MS and MS/MS, 10 ppm and 0.6 Da; maximum missed cleavages allowed, 2.
390 Methionine oxidation and N-acetylation were set as variable modifications, and cysteine
391 carbamidomethylation was set as a fixed modification. A target-decoy database search was
392 used to estimate the false-positive ratio for peptide identification; the false discovery rate
393 was set at 1%.

394

395 **Western blot analysis**

396 Western blot analysis was performed as previously described, with some modifications^{30,31}.
397 Tissues from the brain and peripheral organs were collected from adult c57BL6/J mice,
398 snap-frozen in liquid nitrogen, and stored at -80°C until further use. Peritoneal cavity cells
399 were collected from adult C67BL/6J mice and used as a macrophage sample. Tissues and
400 cultured cells were homogenized in lysis buffer (MCL1, Merck). Protein homogenates were

401 separated with gel electrophoresis using NuPAGE™ 4–12% Bis-Tris gels (Thermo Fisher
402 Scientific) and transferred to polyvinylidene difluoride membranes. Membranes were
403 preincubated in 5% skim milk in Tris-buffered saline with 0.05% Tween® 20 (TBST) for 1 hour
404 and incubated for 2 hours in primary antibody, rabbit polyclonal anti-lactyllysine antibody
405 (PTM Biolabs), or mouse monoclonal anti-β-actin antibody (A5316, Merck) diluted in TBST.
406 They were then incubated for 1 hour with a secondary antibody conjugated with
407 horseradish peroxidase (sc-2357, anti-rabbit IgG; sc-516102, anti-mouse IgG; Santa Cruz
408 Biotechnology) diluted with TBST. All reactions were performed at room temperature.
409 Immunoreactivity was visualized with a chemiluminescence detection reagent (ImmunoStar
410 LD, 292-69903; FUJIFILM Wako Pure Chemical Corporation, Osaka, Japan) and
411 photographed with a luminescent image analyzer (LAS-4000 mini; GE Healthcare,
412 Buckinghamshire, UK).

413

414 **Electroconvulsive stimulation**

415 The experimental mice were briefly anesthetized with isoflurane, and bilateral
416 electroconvulsive stimulation (ECS; current: 25 mA; shock duration: 1 s; frequency: 100
417 pulses/sec; pulse width: 0.5 msec) was administered via ear clip electrodes with a pulse
418 generator (ECT Unit; Ugo Basile, Gemonio, VA, Italy)³⁴. Control mice were handled similarly,
419 except that they were not administered ECS.

420

421 **Chronic SDS**

422 *Condition 1*

423 SDS serves as a preclinical model of chronic stress^{35,36}. We performed chronic social defeat
424 stress in mice at Fujita Health University, as previously described³⁶.

425 *Screening of aggressor ICR mice:* Retired ICR breeders were screened for aggressive
426 behavior for 3 consecutive days. They were individually housed in a clear rectangular
427 hamster cage (26.7 cm [width] × 48.3 cm [depth] × 15.2 cm [height]; Allentown Caging
428 Equipment, Allentown, NJ, USA) equipped with a clear perforated Plexiglass divider (0.6 cm

429 [width] × 45.7 cm [depth] × 15.2 cm [height]; Chubu Kagaku Shizai [custom order]) and a
430 steel-wire top (Allentown Caging Equipment).

431 *Chronic SDS*: Experimental C57BL/6J mice were placed in the compartment containing an
432 aggressor ICR mouse and were exposed to social defeat for 10 minutes. During this period,
433 the experimental mice generally displayed submissive behaviors. They were then
434 transferred to the other compartment of the aggressor's cage, allowing sensory interaction
435 with the intruder C57BL/6J mouse and resident ICR aggressor mouse for approximately 24
436 hours (cohabitation housing condition). This procedure was repeated for 10 consecutive
437 days, with each experimental C57BL/6J mouse being exposed to a novel ICR aggressor each
438 day to prevent habituation. Control C57BL/6J mice were placed in pairs in an identical home
439 cage separated by a perforated divider. The control animals were rotated to a new cage
440 compartment daily and allowed to interact with a novel mouse of the same strain. Following
441 the last defeat session, all C57BL/6J mice were singly housed in standard mouse cages.
442 Twenty-four hours after the last defeat session, a social avoidance test and other behavioral

443 tests were conducted as described. Brain sampling was performed 8 days after the last
444 defeat session. *Condition 1* was used for OX-treatment experiments.

445

446 *Condition 2*

447 The experiment was performed at Fujita Health University, as described in *Condition 1*,
448 except that the intruder C57BL/6J mice were individually housed in separate cages, away
449 from ICR aggressor mice, after the 10-minute-aggression (separation housing condition). As
450 in *Condition 1*, brain sampling was performed 8 days after the last defeat session.

451

452 *Condition 3*

453 The experiment was performed at Ibaraki University, as previously described³⁷. The intruder
454 C57BL/6J mice were exposed to sensory interaction with a resident ICR aggressor mouse in
455 the other compartment of the aggressor's cage for approximately 24 hours (cohabitation

456 housing condition). Twenty-four hours after the last defeat session, a social avoidance test
457 was conducted³⁷. Brain sampling was performed 2 days after the last defeat session.

458

459 **Drug treatment**

460 Twenty minutes prior to each defeat session, the mice were intraperitoneally administered
461 sodium oxamate (OX; 1 g/kg; O2751, Sigma-Aldrich, Tokyo, Japan) or sodium L-lactate (1
462 g/kg; L-7022, Sigma-Aldrich). They were administered the same amount of saline as the
463 control. OX is an inhibitor of lactate dehydrogenase (LDH) activity in the central nervous
464 system^{13,14}. The dose of OX that we used was previously shown to be effective in
465 suppressing seizures in a mouse model of epilepsy¹⁴. The dose of sodium L-lactate that we
466 used was previously shown to exert antidepressant-like effects in a corticosterone-induced
467 chronic stress model in mice⁷.

468

469 **Behavioral tests**

470 Most of the behavioral tests were performed as described elsewhere^{38–41}, unless otherwise
471 noted.

472

473 *Social interaction test*: Social interaction was tested 1 day after the last defeat session as
474 previously described³⁶, with minor modifications. We used an open field chamber (40 cm
475 (width) × 40 cm (depth) × 30 cm (height); O'HARA & Co., Tokyo, Japan) and a wire mesh
476 cage (10.5 cm (width) × 6.5 cm (depth) × 29 cm (height); O'HARA & Co.) to enclose the ICR
477 aggressor mouse. The ICR aggressor mouse that is novel to the defeated C57BL/6J mouse
478 was used. Each social interaction test was composed of two 150-second phases: the ICR
479 aggressor mouse is absent and present in the interaction zone for the first and second phase,
480 respectively. An identical, empty wire mesh cage was placed for the first phase testing. A
481 13.7 cm × 23.6 cm rectangular zone including the wire mesh cage was defined as the social
482 interaction zone. Mouse behaviors were video-monitored, and the trajectory of mouse
483 ambulation, distance traveled, and time spent in the interaction zone for all test phases
484 were automatically determined using ImageSI (see "Image analysis"). A social interaction

485 ratio was calculated by dividing the time spent in the interaction zone when the target was
486 present by the time spent in the interaction zone when the target was absent. A social
487 interaction ratio of 1 was considered the threshold for dividing defeated mice into the
488 susceptible and resilient groups.

489

490 *Light/dark transition test:* A light/dark transition test was conducted as previously
491 described^{38–42}. The apparatus consisted of a cage (42 cm (width) × 21 cm (depth) × 25 cm
492 (height)) divided into two sections of equal size by a partition with a door (O’HARA & Co.).
493 One chamber was brightly illuminated (390 lux), whereas the other chamber was dark (2
494 lux). Mice were placed into the dark chamber and allowed to move freely between the two
495 chambers with the door open for 10 minutes. The total number of transitions, latency to
496 first enter the lit chamber, distance traveled, and time spent in each chamber were
497 recorded using ImageLD (see “Image analysis”).

498

499 *Open field test*: The apparatus was a transparent square cage (42 cm (width) × 42 cm (depth)
500 × 30 cm (height)) equipped with infrared photobeam sensors (VersaMax; Accuscan
501 Instruments, Columbus, OH, USA) with a white floor^{38–41}. The center of the floor was
502 illuminated at 100 lux. Each mouse was placed in the corner of the cage. The total distance
503 traveled (cm), vertical activity (rearing measured by counting the number of photobeam
504 interruptions), time spent in the center area (20 cm × 20 cm), and stereotypic counts
505 (defined by the number of breaks of the same beam) were recorded for 30 minutes using
506 the VersaMax system.

507

508 *Porsolt forced-swim test*: A Plexiglas cylinder (20 cm height × 11.4 cm diameter; O'HARA &
509 Co.) filled with water (21–23 °C) up to a height of 8 cm was placed in a white plastic chamber
510 (32 cm (width) × 44 cm (depth) × 49 cm (height); O'HARA & Co.)^{38–41}. Mice were placed into
511 the cylinder, and both immobility and distance traveled were recorded over a 10-minute
512 test period. The test was conducted for 2 consecutive two days, and the results of the first
513 trial are shown. Images were captured at two frames per second. For each pair of successive

514 frames, the amount of area (pixels) in which the mouse moved was measured. When the
515 amount of area was below a certain threshold, mouse behavior was classified as “immobile.”
516 When the amount of area equaled or exceeded the threshold, the mouse was classified as
517 “moving”. The optimal threshold to judge movement was determined by adjusting it to the
518 amount of immobility measured by human observation. Immobility lasting for less than 2
519 seconds was not included in the analysis. Data acquisition and analysis were performed
520 automatically, using ImagePS/TS (see “Image analysis”).

521

522 *Tail suspension test*: Each mouse was suspended 30 cm above the floor by the tail in a white
523 plastic chamber (41cm (width) × 31 cm (depth) × 41 cm (height); O’Hara & Co.)^{38–41}. The
524 behavior was recorded for 10 minutes. Images were captured through a video camera, and
525 immobility was measured. Similar to the Porsolt forced swim test mentioned above,
526 immobility was judged using ImagePS/TS (see “Image analysis”) according to a certain
527 threshold. Immobility lasting <2 seconds was not included in the analysis.

528

529 *Sucrose preference test*: C57BL/6J mice were subjected to a two-bottle choice test, in which
530 mice were provided with a bottle containing water and a second bottle containing 1%
531 sucrose solution, with the left/right positions of the bottles counterbalanced across groups
532 ^{39,40}. The mice were habituated to a two-bottle condition during all the experimental period.
533 Sucrose preference during 4-hour in the test day was calculated as the percentage of
534 sucrose preference = $100 \times \{[\text{sucrose intake (g)}]/(\text{sucrose intake (g)} + \text{water intake (g)})\}$.

535

536 *Locomotor activity monitoring in the home cage*: Locomotor activity monitoring in the home
537 cage was performed as previously described^{30,41}. A system that automatically analyzes the
538 locomotor activity of mice in their home cage was used⁴³. The system contains a home cage
539 (29 cm (width) × 18 cm (depth) × 12 cm (height)) and filtered cage top, separated by a 13-
540 cm-high metal stand containing an infrared video camera, attached to the top of the stand.
541 Each mouse was individually housed in each home cage, and their locomotor activity was
542 monitored for 6 days. Mice were allowed to habituate to the test apparatus, and hence, the

543 data of the latter 3 days were analyzed. Distance traveled was measured automatically
544 using ImageHA (see “Image analysis”).

545

546 *Image analysis*: For the social interaction test, light/dark transition test, Porsolt forced swim
547 test, and tail suspension test, image analysis programs (ImageSI/LD/PS/TS/HA) were used
548 to automatically analyze mouse behaviors. The application programs, based on the public
549 domain ImageJ program (developed by Wayne Rasband at the National Institute of Mental
550 Health, Bethesda), were developed and modified for each test by Tsuyoshi Miyakawa.
551 ImageLD program can be freely downloaded from the website of the “Mouse Phenotype
552 Database” (<http://www.mouse-phenotype.org/>)⁴⁴.

553

554 **Measurements of brain lactate levels and pH**

555 In the *in vivo* experiments, the whole brain was used to measure tissue pH and lactate levels
556 as previously described³. Briefly, snap-frozen tissues were homogenized in ice-cold distilled

557 H₂O (5 mL per 500 mg of tissue). The pH of the homogenates was measured using a pH
558 meter (LAQUA F-72, HORIBA, Ltd., Kyoto, Japan) equipped with a Micro ToupH electrode
559 (9618S-10D, HORIBA, Ltd.) after a three-point calibration at pH 4.0, 7.0, and 9.0. Following,
560 the concentration of lactate in the homogenates was determined using a multi-assay
561 analyzer (GM7 Micro-Stat; Analox Instruments Ltd., London, UK) after calibration with an
562 8.0-M standard lactate solution (GMRD-103, Analox Instruments). A 20- μ L aliquot of
563 centrifuged supernatant was used for the measurement. In the *in vitro* experiments, lactate
564 concentrations of the cultured cells and culture supernatant were measured using the
565 lactate colorimetric assay kit II (K627-100; BioVision, Milpitas, CA, USA). Light transmittance
566 was measured at a wavelength of 450 nm using a spectrophotometer (DU730; Beckman
567 Coulter, Tokyo, Japan).

568

569 **Statistical analysis**

570 The data were analyzed by Student's t-test, one-way analysis of variance (ANOVA), two-way
571 ANOVA, followed by Tukey's honestly significant difference post-hoc test, or linear

572 regression analysis using R version 3.5.2 or SAS Studio software version 9.4 (SAS Institute
573 Inc., Cary, NC, USA).

574

575 **Data availability**

576 The original blot images are provided in Extended data figures. The full statistical results are
577 provided in Extended data tables.

578

579 **References**

- 580 1. Zhang, D. *et al.* Metabolic regulation of gene expression by histone lactylation.
581 *Nature* **574**, 575–580 (2019).
- 582 2. Magistretti, P. J. & Allaman, I. Lactate in the brain: from metabolic end-product
583 to signalling molecule. *Nat. Rev. Neurosci.* **19**, 235–249 (2018).
- 584 3. Hagihara, H. *et al.* Decreased brain pH as a shared endophenotype of psychiatric
585 disorders. *Neuropsychopharmacology* **43**, 459–468 (2018).
- 586 4. Hagihara, H. *et al.* Systematic analysis of brain lactate and pH levels in 65 animal
587 models related to neuropsychiatric conditions. *bioRxiv* 2021.02.02.428362 (2021).
- 588 5. Irizarry-Caro, R. A. *et al.* TLR signaling adapter BCAP regulates inflammatory to
589 reparatory macrophage transition by promoting histone lactylation. *Proc. Natl. Acad. Sci.*
590 **117**, 30628–30638 (2020).

- 591 6. Cui, H. *et al.* Lung myofibroblasts promote macrophage profibrotic activity
592 through lactate-induced histone lactylation. *Am. J. Respir. Cell Mol. Biol.* **64**, 115–125
593 (2020).
- 594 7. Carrard, A. *et al.* Peripheral administration of lactate produces antidepressant-
595 like effects. *Mol. Psychiatry* (2016) doi:10.1038/mp.2016.179.
- 596 8. Busnello, J. V. *et al.* Acute and chronic electroconvulsive shock in rats: Effects on
597 peripheral markers of neuronal injury and glial activity. *Life Sci.* **78**, 3013–3017 (2006).
- 598 9. Díaz-García, C. M. *et al.* Neuronal stimulation triggers neuronal glycolysis and
599 not lactate uptake. *Cell Metab.* **26**, 361–374.e4 (2017).
- 600 10. Lazeyras, F. *et al.* MRI, 1H-MRS, and functional MRI during and after prolonged
601 nonconvulsive seizure activity. *Neurology* **55**, 1677–1682 (2000).
- 602 11. Najm, I. M. *et al.* Temporal changes in proton MRS metabolites after kainic acid-
603 induced seizures in rat brain. *Epilepsia* **38**, 87–94 (1997).
- 604 12. Oses, J. P. *et al.* Sustained elevation of cerebrospinal fluid glucose and lactate
605 after a single seizure does not parallel with mitochondria energy production. *Epilepsy Res.*
606 **152**, 35–41 (2019).
- 607 13. Lam, T. K. T., Gutierrez-Juarez, R., Pocai, A. & Rossetti, L. Regulation of blood
608 glucose by hypothalamic pyruvate metabolism. *Science* **309**, 943–947 (2005).
- 609 14. Sada, N., Lee, S., Katsu, T., Otsuki, T. & Inoue, T. Targeting LDH enzymes with a
610 stiripentol analog to treat epilepsy. *Science* **347**, 1362–1367 (2015).
- 611 15. Bullitt, E. Expression of C-fos-like protein as a marker for neuronal activity
612 following noxious stimulation in the rat. *J. Comp. Neurol.* **296**, 517–530 (1990).
- 613 16. Bullitt, E., Lee, C. L., Light, A. R. & Willcockson, H. The effect of stimulus duration
614 on noxious-stimulus induced c-fos expression in the rodent spinal cord. *Brain Res.* **580**,
615 172–179 (1992).
- 616 17. Kollack-Walker, Don, Watson, & Akil. Differential Expression of c- fos mRNA
617 Within Neurocircuits of Male Hamsters Exposed to Acute or Chronic Defeat. *J.*
618 *Neuroendocrinol.* **11**, 547–559 (1999).
- 619 18. Martinez, M., Calvo-Torrent, A. & Herbert, J. Mapping brain response to social
620 stress in rodents with c-fos expression: A review. *Stress* **5**, 3–13 (2002).

- 621 19. Matsuda, S. *et al.* Persistent c-fos expression in the brains of mice with chronic
622 social stress. *Neurosci. Res.* **26**, 157–170 (1996).
- 623 20. Ma, M. *et al.* Adjunctive treatment of brexpiprazole with fluoxetine shows a
624 rapid antidepressant effect in social defeat stress model: Role of BDNF-TrkB signaling. *Sci.*
625 *Rep.* **6**, 1–12 (2016).
- 626 21. Yang, B. *et al.* Comparison of R-ketamine and rapastinel antidepressant effects
627 in the social defeat stress model of depression. *Psychopharmacology (Berl.)* **233**, 3647–
628 3657 (2016).
- 629 22. Huang, D. W., Sherman, B. T. & Lempicki, R. A. Systematic and integrative
630 analysis of large gene lists using DAVID bioinformatics resources. *Nat. Protoc.* **4**, 44–57
631 (2009).
- 632 23. Huang, D. W., Sherman, B. T. & Lempicki, R. A. Bioinformatics enrichment tools:
633 paths toward the comprehensive functional analysis of large gene lists. *Nucleic Acids Res.*
634 **37**, 1–13 (2009).
- 635 24. Martinez, M., Phillips, P. J. & Herbert, J. Adaptation in patterns of c-fos
636 expression in the brain associated with exposure to either single or repeated social stress
637 in male rats. *Eur. J. Neurosci.* **10**, 20–33 (1998).
- 638 25. Gaffney, D. O. *et al.* Non-enzymatic lysine lactoylation of glycolytic enzymes. *Cell*
639 *Chem. Biol.* **27**, 206–213.e6 (2020).
- 640 26. Andrés, M., García-Gomis, D., Ponte, I., Suau, P. & Roque, A. Histone H1 post-
641 translational modifications: update and future perspectives. *Int. J. Mol. Sci.* **21**, 5941
642 (2020).
- 643 27. Wisniewski, J. R., Zougman, A., Krüger, S. & Mann, M. Mass spectrometric
644 mapping of linker histone H1 variants reveals multiple acetylations, methylations, and
645 phosphorylation as well as differences between cell culture and tissue. *Mol. Cell.*
646 *Proteomics MCP* **6**, 72–87 (2007).
- 647 28. Kamieniarz, K. *et al.* A dual role of linker histone H1.4 Lys 34 acetylation in
648 transcriptional activation. *Genes Dev.* **26**, 797–802 (2012).
- 649 29. Anti-L-lactyllysine rabbit pAb. *PTM BIO*
650 <https://www.ptmbiolabs.com/product/anti-lactyllysine-rabbit-pab/> (2019).

- 651 30. Hagihara, H. *et al.* Circadian gene circuitry predicts hyperactive behavior in a
652 mood disorder mouse model. *Cell Rep.* **14**, 2784–2796 (2016).
- 653 31. Hagihara, H., Ohira, K., Toyama, K. & Miyakawa, T. Expression of the AMPA
654 receptor subunits GluR1 and GluR2 is associated with granule cell maturation in the
655 dentate gyrus. *Front. Neurosci.* **5**, (2011).
- 656 32. Franklin, K. B. J. & Paxinos, G. *The Mouse Brain in Stereotaxic Coordinates*.
657 (Academic Press Inc.. San Diego., 1997).
- 658 33. Tanaka, M. *et al.* Fascin in lamellipodia contributes to cell elasticity by
659 controlling the orientation of filamentous actin. *Genes Cells* **24**, 202–213 (2019).
- 660 34. Imoto, Y., Segi-Nishida, E., Suzuki, H. & Kobayashi, K. Rapid and stable changes in
661 maturation-related phenotypes of the adult hippocampal neurons by electroconvulsive
662 treatment. *Mol. Brain* **10**, 8 (2017).
- 663 35. Krishnan, V., Berton, O. & Nestler, E. The use of animal models in psychiatric
664 research and treatment. *Am. J. Psychiatry* **165**, 1109 (2008).
- 665 36. Golden, S. A., Covington, H. E., Berton, O. & Russo, S. J. A standardized protocol
666 for repeated social defeat stress in mice. *Nat. Protoc.* **6**, 1183–1191 (2011).
- 667 37. Goto, T. *et al.* Subchronic and mild social defeat stress accelerates food intake
668 and body weight gain with polydipsia-like features in mice. *Behav. Brain Res.* **270**, 339–348
669 (2014).
- 670 38. Shoji, H. & Miyakawa, T. Age-related behavioral changes from young to old age
671 in male mice of a C57BL/6J strain maintained under a genetic stability program.
672 *Neuropsychopharmacol. Rep.* **39**, 100–118 (2019).
- 673 39. Shoji, H. & Miyakawa, T. Increased depression-related behavior during the
674 postpartum period in inbred BALB/c and C57BL/6 strains. *Mol. Brain* **12**, 70 (2019).
- 675 40. Shoji, H. & Miyakawa, T. Differential effects of stress exposure via two types of
676 restraint apparatuses on behavior and plasma corticosterone level in inbred male
677 BALB/cAJcl mice. *Neuropsychopharmacol. Rep.* **40**, 73–84 (2020).
- 678 41. Nakajima, R. *et al.* Comprehensive behavioral analysis of heterozygous Syngap1
679 knockout mice. *Neuropsychopharmacol. Rep.* **39**, 223–237 (2019).

680 42. Takao, K. & Miyakawa, T. Light/dark transition test for mice. *J. Vis. Exp. JoVE* 104
681 (2006) doi:10.3791/104.

682 43. Miyakawa, T. *et al.* Conditional calcineurin knockout mice exhibit multiple
683 abnormal behaviors related to schizophrenia. *Proc. Natl. Acad. Sci. U. S. A.* **100**, 8987–
684 8992 (2003).

685 44. Hattori, S., Okumura, Y., Takao, K., Yamaguchi, Y. & Miyakawa, T. Open source
686 code for behavior analysis in rodents. *Neuropsychopharmacol. Rep.* **39**, 67–69 (2019).

687

688 **Acknowledgements**

689 We thank Giovanni Sala for invaluable comments on statistics. We also thank Tamaki

690 Murakami, Chikako Ozeki, Wakako Hasegawa, Yumiko Mobayashi, Yoko Kagami, Harumi

691 Mitsuya, Yoshihiro Takamiya, Satoko Hattori and Miho Tanaka for their technical assistance.

692 This work was supported by MEXT KAKENHI Grant Number JP16H06462, JP17H06417, and

693 JP17H06413, MEXT Promotion of Distinctive Joint Research Center Program Grant Number

694 JPMXP0618217663, JSPS KAKENHI Grant Number JP20H00522, JP18K07378, JP19K06502,

695 and JP16H06276 (AdAMS), and AMED Strategic Research Program for Brain Sciences Grant

696 Number JP18dm0107101.

697

698 **Author information**

699 **Contributions.** H.H. and T.M. designed experiments. H.H. wrote the manuscript. K.N., K.K.,
700 and T.M. helped draft the manuscript. H.H., H.S., H.O., and A.T. performed the behavioral
701 tests and analyzed the data. K. K. and M. N. performed STED microscopy analysis. T.M.
702 supervised all aspects of the present study. All authors have approved the final manuscript.

703 **Corresponding authors.** Correspondence to Tsuyoshi Miyakawa.

704

705 **Ethics declarations**

706 The authors declare no competing interests.

707 **Figure legends**

708 **Figure 1. Protein lactylation induced by exogenous lactate in brain cells.** (a) Western blot
709 images of lactylated lysine (Kla) in mouse tissues/cells (hippocampus (HIP), cerebral cortex
710 (CX), and resident macrophages (MP). Entire membrane images are provided in the
711 Extended Data Fig. 1. (b) Double immunostaining for Kla and the neuronal marker β III-
712 tubulin in primary cultured cortical neurons (10 days in vitro, DIV). Scale bar: 20 μ m. (c, d)
713 Kla levels in primary cultured cortical neurons (10 DIV) examined 30 minutes after
714 treatment with lactate (25 mM, +) and/or 4-CIN (0.01 mM, +; 1 mM, ++) using
715 immunocytochemistry. Arrow in (c) indicates the sampling time point. At least 200 cells
716 were examined for each condition. Statistical results are provided in Extended Data Table
717 4. (e) Glial fibrillary acidic protein (GFAP) and Kla double immunostaining at 10 DIV in culture.
718 Open arrows indicate GFAP-positive astrocyte-like cells. Solid arrows indicate GFAP-
719 negative neuronal cells. Scale bar: 50 μ m. (f–h) Mice were intraperitoneally injected with 1
720 g/kg lactate or saline, once daily for 21 days. (g) Kla immunostaining images of the
721 prefrontal cortices (PFCs) of control and lactate-treated mice. Scale bar: 100 μ m. (h) Bar

722 graph showing Kla immunoreactivity levels of the PFC of control and lactate-treated mice
723 (P = 0.022, n = 7, 6). (i) Mouse PFC: Double immunostaining images of Kla and the
724 glutamatergic neuron marker Camk2a (upper left panel), the GABAergic neuron marker
725 GAD67 (upper right panel), the astrocyte marker S100b (lower left panel), and the microglial
726 marker CD68 (lower right panel). Scale bar: 25 μ m.

727

728 **Figure 2. Neuronal excitation stimulates protein lactylation in neurons.** (a–c) Primary
729 cultured cortical neurons (10 DIV) were treated with potassium chloride (KCl), with or
730 without sodium oxamate (OX). Arrows indicate sampling time points (a). Cultured neurons
731 were treated with KCl (100 mM) and lactate concentrations were measured in the culture
732 supernatant (upper panel, b) and cell lysate (lower panel, b). *P < 0.05, one-way analysis of
733 variance (ANOVA) followed by post-hoc pairwise comparisons. N = 5 for each condition.
734 Statistical results are provided in the Extended Data Table 5. (c) Results of Kla
735 immunostaining analysis of cultured neurons expressing β III-tubulin treated with KCl [10
736 mM (+) or 100 mM (++)] and OX [20 mM (+)] (c) At least 300 cells were examined for each

737 condition. ****P** < 0.01; **##P** < 0.01 compared to the KCl/OX condition; one-way ANOVA
738 followed by post-hoc pairwise comparisons (Extended Data Table 6). (d, e) Brain lactate
739 levels in mice treated with electroconvulsive stimulation (ECS) (N = 8 mice for each
740 condition). **##P** < 0.01 compared to control; one-way ANOVA followed by post-hoc pairwise
741 comparisons (Extended Data Table 7). (f–h) K_{la} in the mouse brain treated with ECS. Adult
742 mice were treated with ECS 30 minutes after treatment with OX, α -cyano-4-
743 hydroxycinnamate (4-CIN), or saline. Brain sampling was performed 1 hour after ECS
744 treatment (arrow, f). Immunostaining images of K_{la} in the prefrontal cortex (PFC). Scale bar:
745 100 μ m (g). Graph showing K_{la} immunoreactivity in the PFCs of the mice (h). **#P** < 0.05
746 compared to ECS-/OX-/4-CIN-, **\$P** < 0.05 compared to ECS+/OX-/4-CIN-; one-way ANOVA
747 followed by post-hoc pairwise comparisons. N = 6–7 mice for each condition (Extended Data
748 Table 8). (i) K_{la} and c-Fos double immunostaining images of the mouse PFC at 1 hour after
749 an ECS. Open and solid arrowheads indicate cells with low and high levels of K_{la} + c-Fos,
750 respectively. Scale bar: 50 μ m. (j) Scatterplot showing a correlation between K_{la} and c-Fos
751 immunoreactivity in individual cells in the PFC (represented as Z-score transformed values).

752 Data from 543 cells from 15 mice in four different conditions (Extended Data Fig. 4) are
753 integrated in the graph.

754

755 **Figure 3. Social stress induces protein lactylation in the brain.** (a–c) Mice were exposed to
756 repeated social defeat stress, with or without sodium oxamate injections and then analyzed
757 by a series of behavioral tests (a). Arrow in (a) indicates the sampling time point. FS: Porsolt
758 forced swim test; LD: light-dark transition test; OF: open field test; OX: sodium oxamate; SA:
759 social avoidance test; SDS: social defeat stress; SP: sucrose preference test; TS: tail
760 suspension test. (b) Social avoidance test. (c) Brain lactate levels in the three groups of mice.
761 N = 10–14 mice for each condition. Statistical results are provided in the Extended Data
762 Table 9 and 10, respectively. (d) Correlation matrix showing correlation coefficients
763 between behavioral measures and brain lactate levels in control and socially defeated mice.
764 (e, f) Brain sampling for immunohistochemical analysis was performed using another set of
765 mice exposed to SDS with or without OX injection. (e) HC: home cage locomotor activity
766 monitoring test. (f) Immunostaining images of Kla and bar graph showing Kla

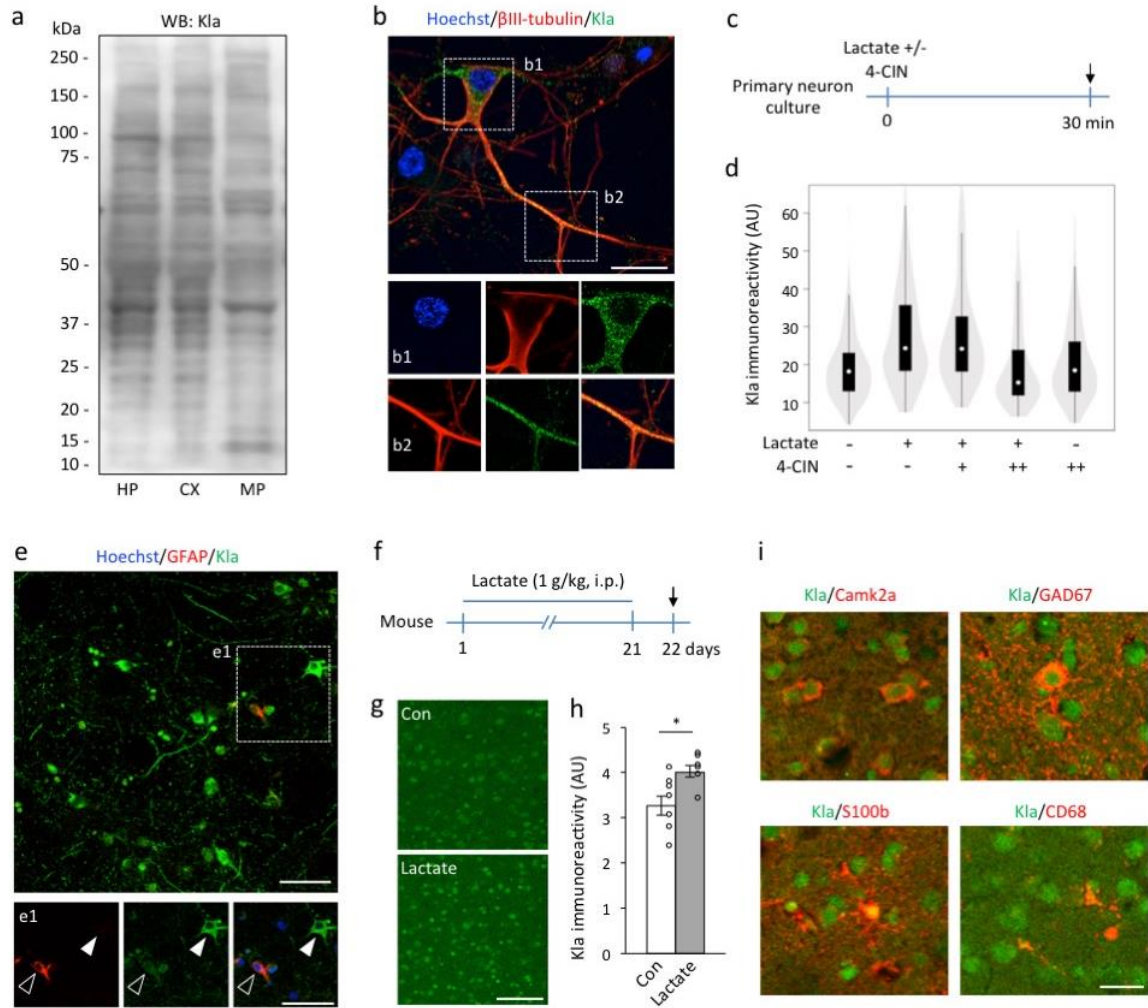
767 immunoreactivity in the prefrontal cortex (PFC). Scale bar: 100 μm . ** $P < 0.01$, one-way
768 analysis of variance followed by post-hoc pairwise comparisons; $N = 6$ mice for each
769 condition (Extended Data Table 11). (g) Immunostaining images of c-Fos in the PFC. (h) Bar
770 graphs showing c-Fos-positive cells in the PFC (Extended Data Table 12). Mice in the home
771 cage group were sampled immediately after being removed from the home cage. Mice in
772 the OF group were sampled after a 2-hour exposure to the open field. (i–k) Scatterplots
773 showing correlations between Kla immunoreactivity and c-Fos expression in the PFC and (i)
774 the social interaction ratio in the social avoidance test (j), and the distance traveled in the
775 dark compartment in the light/dark transition test, in mice from the OF group. $N = 6$ for
776 each condition.

777

778 **Figure 4. Histone H1 lactylation in the brain is increased by social stress.** (a) Double
779 immunostaining of Kla and histone H1 in the mouse PFC. Arrows indicate Kla-negative and
780 histone H1-positive Hoechst-stained cells, and arrowheads indicate Kla-negative and
781 histone H1-negative Hoechst-stained cells. Scale bar: 50 μm . (b) Venn diagram showing the

782 overlap between Kla-positive and histone H1-positive cells in the mouse PFC. (c) Super-
783 resolution images of Kla and histone H1 in the nuclei of neurons of socially defeated mice
784 recorded with STED microscopy. Arrowheads indicate Kla- and histone H1-double-positive
785 structures. Scale bars: 5 μm (upper panels), 1 μm (lower panels). (d) Bar graphs show the
786 percentage of Kla and histone H1 merged area in the nucleus. N = 18 cells from 3 mice for
787 each condition. *P = 0.012, linear regression analysis.
788

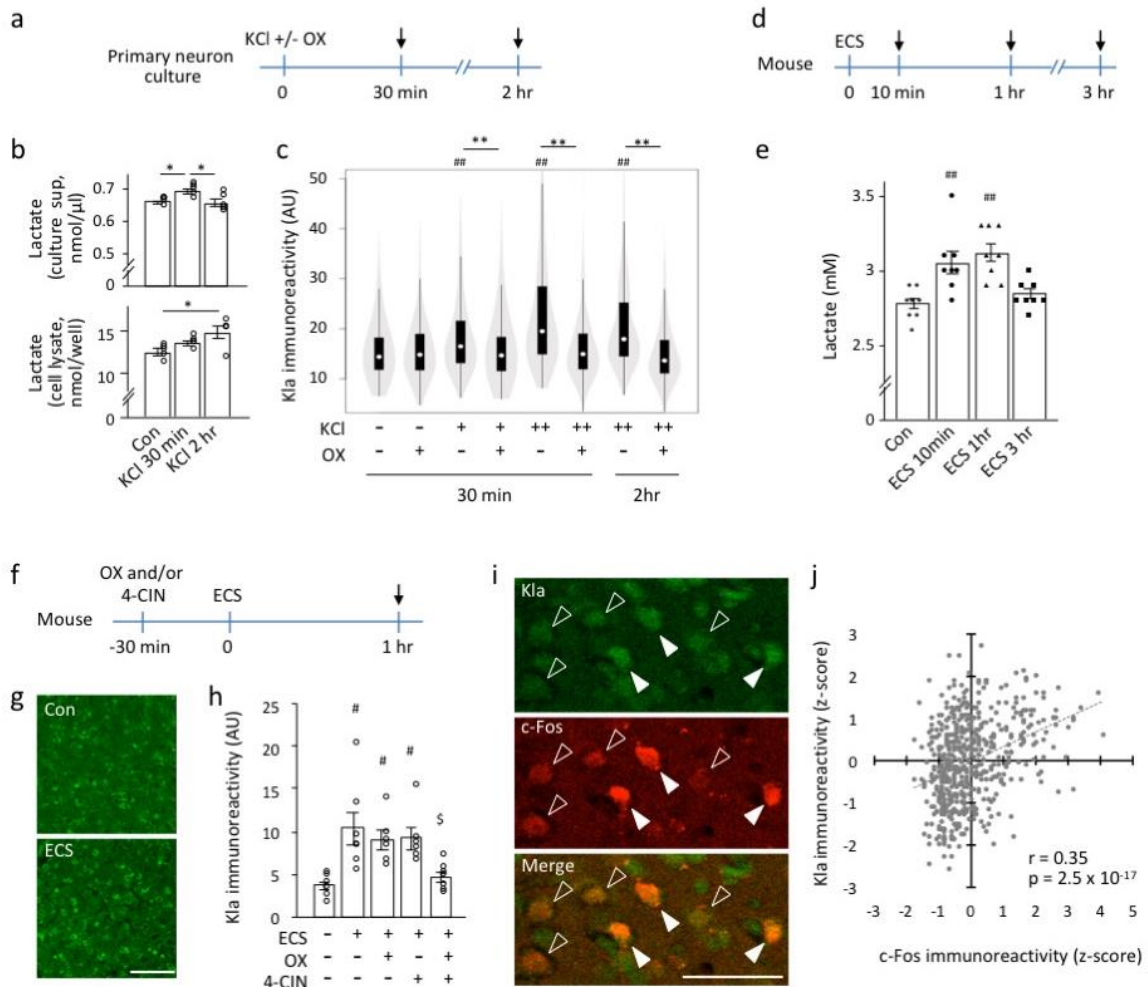
789 Figure 1



790

791

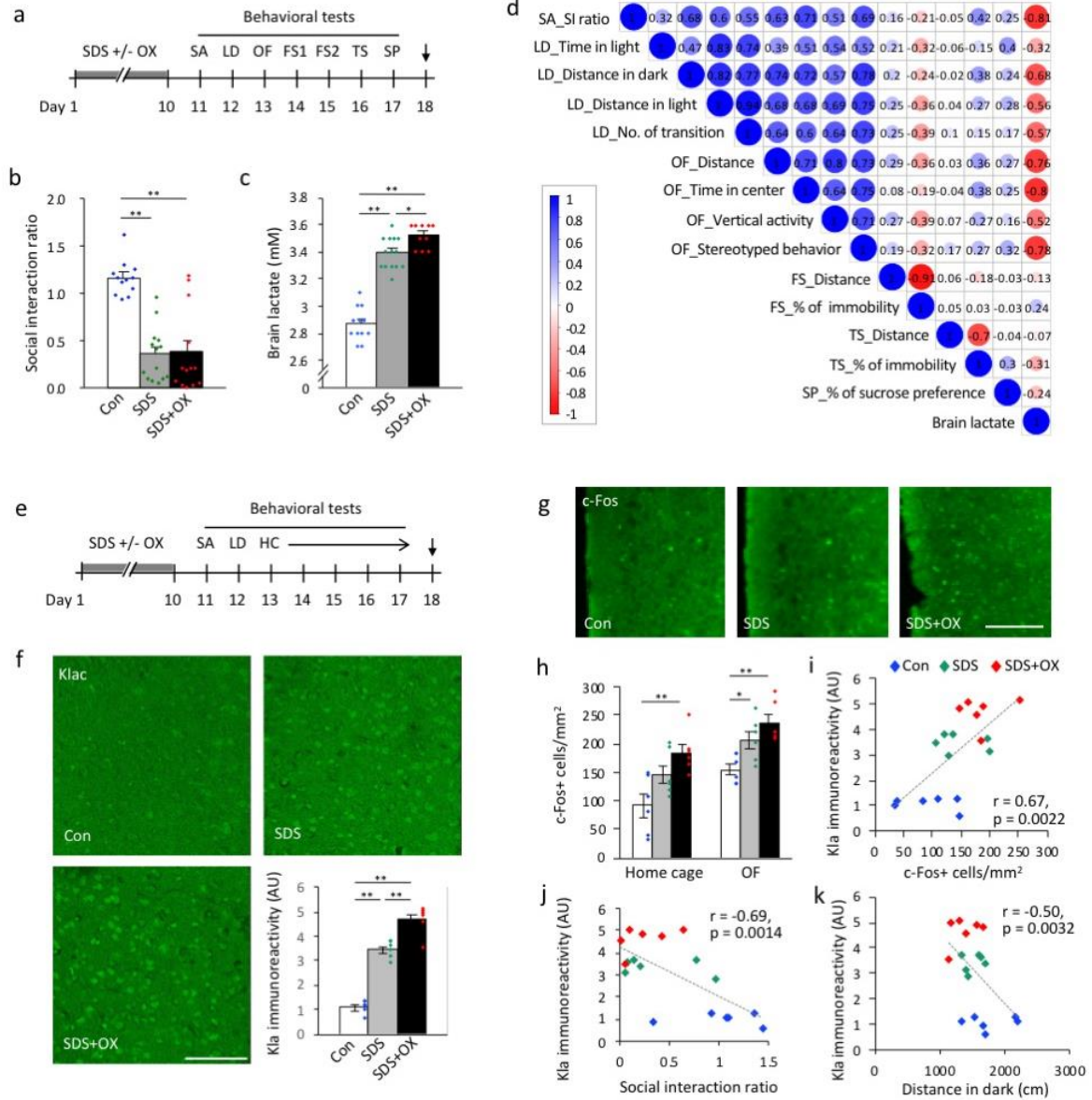
792 Figure 2



793

794

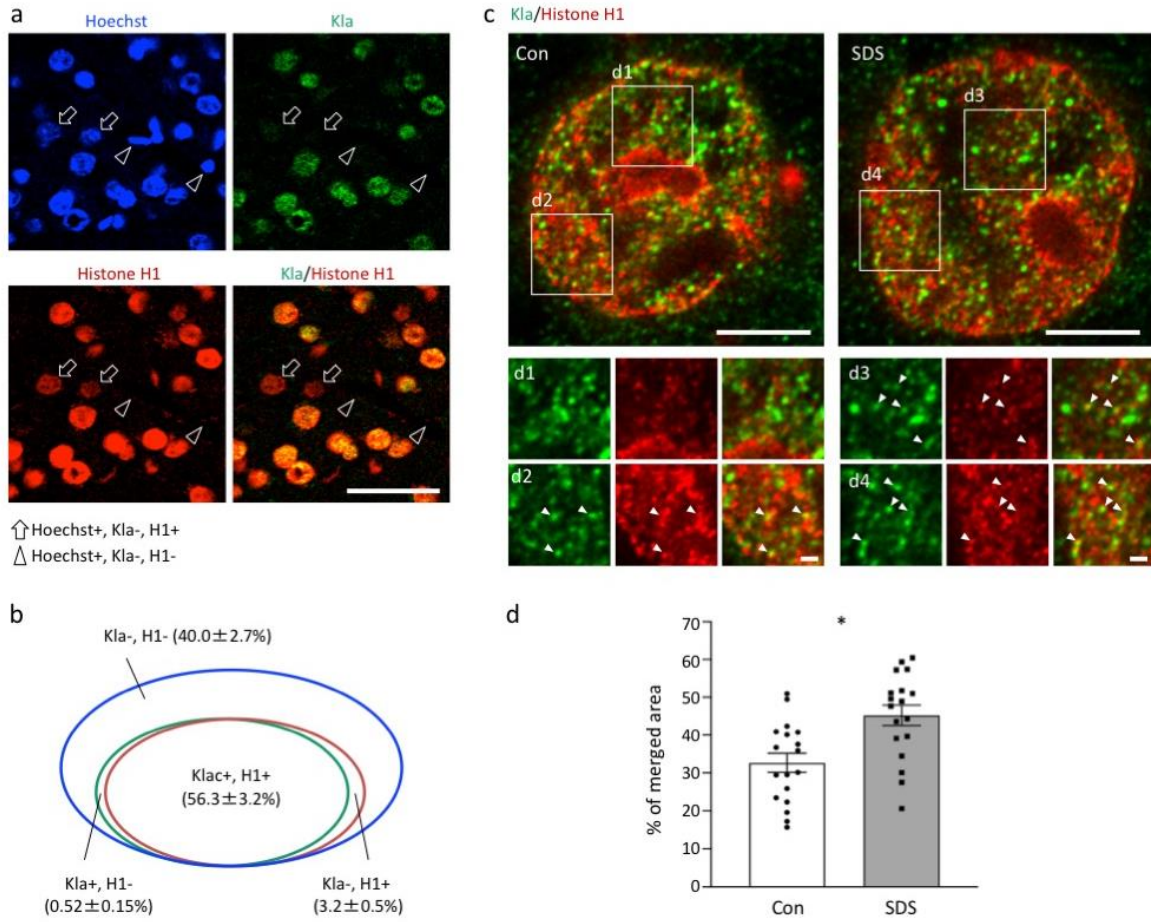
795 Figure 3



796

797

798 Figure 4



799

800